energies

MDPI

Article

New Performance Indices for Power System Stabilizers

Michał Izdebski [1,*], Robert Małkowski [2] and Piotr Miller [3]

[1] Institute of Power Engineering, 01-330 Warszawa, Poland
[2] Department of Electrical Power Engineering, Faculty of Electrical and Control Engineering, Gdansk University of Technology, 80-233 Gdansk, Poland
[3] Department of Power Engineering, Faculty of Electrical Engineering and Computer Science, Lublin University of Technology, 20-618 Lublin, Poland
* Correspondence: m.izdebski@ien.gda.pl

Abstract: The subject of the article is issues related to innovative indices for power system stabilizers (PSSs). These new indices will be able to quickly show which PSS (among many other PSSs) is not working properly and that advanced optimization and simulation methods should be used to improve the PSS settings. The authors note the fact that the acceptance requirements for PSSs are different in various power systems. Moreover, the authors pay attention to the fact that transmission system operators (TSOs) often have different PSS requirements (tests) even though they work in the same large power system. The article reviews the requirements for the PSSs used by TSOs of various power systems. The need to supplement the required tests with new qualitative indices is demonstrated. In the paper, new performance indices are proposed to improve the evaluation of the PSS and to check the desired performance of the stabilizer. These indices are derived from the active power frequency response characteristic with PSS and without PSS (PSS ON and PSS OFF). Additionally, the new PSS indices allow the graphical visualization of the properties of all synchronous generators equipped with the PSS in a predefined area on a single 3D graph. Such visualization can be used to quickly detect weak points of the power system.

Keywords: acceptance requirements; performance index; power system; power system stabilizer

Citation: Izdebski, M.; Małkowski, R.; Miller, P. New Performance Indices for Power System Stabilizers. *Energies* **2022**, *15*, 9582. https://doi.org/10.3390/en15249582

Academic Editor: Anna Pinnarelli

Received: 1 November 2022
Accepted: 13 December 2022
Published: 16 December 2022

1. Introduction

Synchronous generators operate over a wide range of operating conditions with many types of disturbances from the power system. They include, among others, active power oscillations (electromechanical swings of the power system). If appropriate damping is not available in the generator, the active power oscillations due to disturbances that may appear can cause generator tripping or even power-system collapse [1]. To produce a positive damping of these oscillations, an additional regulation loop is used in the synchronous generator's excitation-control system. This loop is called the power system stabilizer (PSS). The PSS can damp the oscillatory modes that involve a small number of generators close to the considered generator, which are called local modes (0.7–3 Hz). Large power systems also experience global oscillatory phenomena that involve a large number of generators and are characterized by the inter-area modes (0–1 Hz) [2]. A fine-tuned PSS should have adequate damping of local modes and also provide damping of inter-area modes (damping of the active power response tested in the frequency domain and in the time domain [1]). Furthermore, a fine-tuned PSS is very important due to the fact that it can damp the oscillations or the opposite effect will occur, which may have fatal consequences for the stability of the power system. Therefore, the PSS is an important element for the stability of the power system.

An increase in generation from renewable energy sources; e.g., wind farms or photovoltaic installations, contributes to a reduction in the inertia constant of a power system and the transient stability issues [3]. The reduction in stored kinetic energy (inertia) will

have an effect on system operation and security due to an increase in the amplitudes of the frequency variations [1]. Additionally, an increase in photovoltaic installations in the power system decreases the damping of the inter-area oscillation mode. The mode shape varies with the photovoltaic control strategy, and new oscillation modes may occur under inappropriate parameter settings in the photovoltaic plant controls [4]. So, the importance of the PSS is growing.

Research work related to power system stabilizers can be divided into two main groups. The first group of publications covers issues related to the optimization of PSSs [5–7]. The second group is searching for new PSS structures [8]. The spectrum of the proposed PSS tuning techniques is very wide and includes conventional tuning methods [9–11], heuristic methods [12], neural networks [13], mixed target functions [14], and finally artificial intelligence [15]. Many methods can be used to numerically solve the problem of multi-criteria optimization [16] and the problem of the correct location of the PSS [17]. The above-mentioned algorithms mainly regard optimization, but the subject of this article was to develop "quick" indices to show if a PSS is working properly.

To check the correctness of PSS settings, it would be best to use optimization algorithms [5–7,16] that are verified in each case by a simulation study. Unfortunately, these are time-consuming and costly. Bearing the above in mind, we propose the use of two new indices that can verify the correctness of PSS tuning faster and easier. The indices do not require costly and complex tests. The effectiveness of the proposed PSS indices have been practically demonstrated for the selected generating units in the power system based on real measurements made by one of this paper's authors. The new indices will make it possible to compare the effectiveness of PSSs in a close location in a power system (managed by the same TSO) and indicate the PSS with the worst settings—which can be further analyzed using advanced optimization algorithms.

Unfortunately, the acceptance requirements for PSSs are different in other power systems. It is also worth noting that transmission system operators (TSOs) have different requirements (tests) even though they work in the same large power system. The PSS requirements include tests such as the following:

- Step-response test,
- Line-switching test,
- Frequency-response test,
- Gain margin,
- Limiting-function test,
- PSS/limiter interaction test,
- Damping index from step-response test.

In these tests, there is only one performance index (damping from step-response test) that clearly describes the quality of the PSS as a numerical value (test details based on TSO requirements are described in Section 5). This fact confirmed that additional PSS indices in the form of a numerical value are also needed.

This paper will be present an overview of how the PSS function is built into the structure of the excitation system, the PSS-P-ω theory, the process of PSS parameter selection, an overview of the PSS tests performed in the world, the PSS performance index used, and new performance indices proposed for the PSS.

Additionally, this paper will describe the practical application of these two new PSS indices. The considerations were limited to the currently recommended dual-input PSS-P-ω stabilizers (industrial standard), which included types PSS2A, PSS2B, and PSS2C [18].

Test systems usually are used to analyze the work of PSSs, but we used the possibility of their practical verification. In our opinion, the tests performed on real objects allowed for a correct and reliable assessment of the new indices' effectiveness and the verification of their practical application.

2. PSS in the Excitation System of the Synchronous Generator

The phrase "excitation system of the synchronous generator" is a kind of simplification. In fact, this system consists of the following two separate elements [19]:

- Synchronous machine regulator (excitation controller),
- Exciter (static or rotating).

The exciter has a subordinate function in relation to the synchronous machine regulator, which is the control unit of the exciter. This relationship is shown in Figure 1.

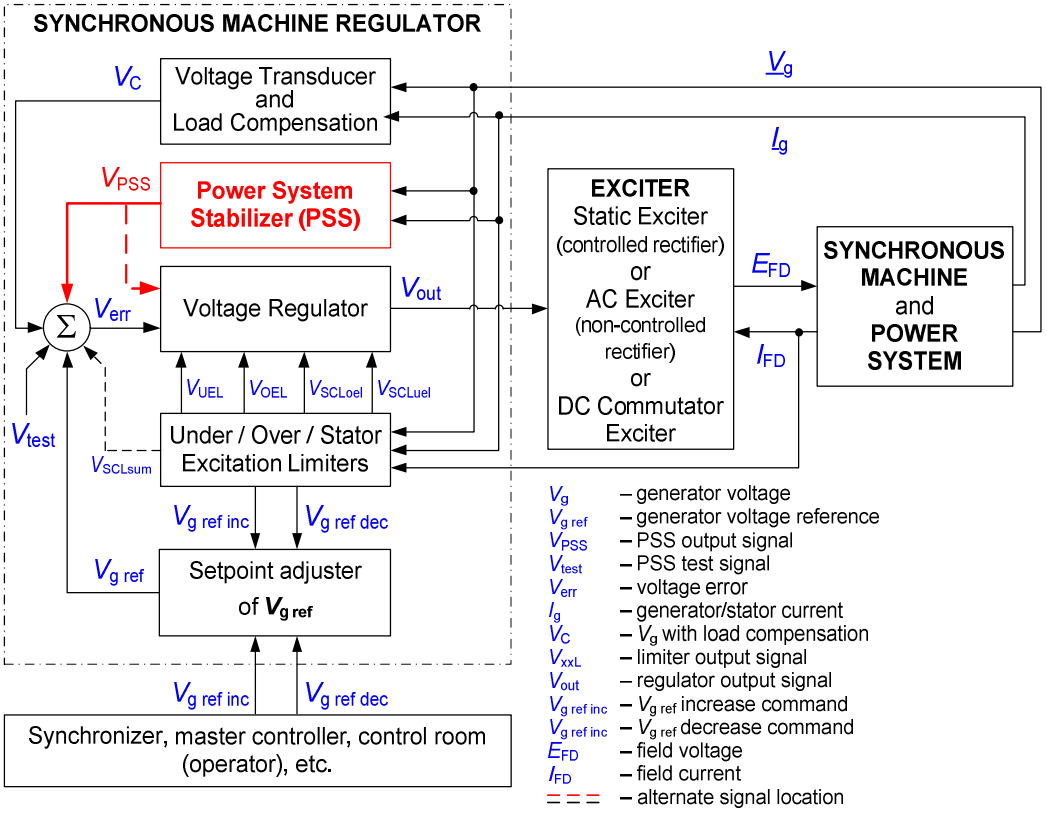

Figure 1. Block diagram of an excitation system.

Modern synchronous machine regulators have many more functions than just regulation of the terminal voltage. The synchronous machine regulator is now synonymous with the digital excitation-control system. These systems have a complex structure, usually dual-channel or even three-channel. Today's regulators must have many additional important functions that allow, among others:

- Cooperation with power plant automation systems [20]—many communication interfaces,
- Detection of thyristor conduction loss [21]—self-diagnostic of the excitation system,
- Measurement of the generator's rotor-winding temperature [22]—generator diagnostics,
- Damping of terminal voltage oscillations or active power oscillations when the generator is driven by a low-speed engine [23] (light-frequency compensator),
- Communication with power plant control systems [24].
- The main functions of synchronous machine regulators are:
- Starting of the excitation system in an open-circuit condition without overshoot of the terminal voltage,
- Terminal voltage regulation, reactive power regulation, or power-factor regulation,
- Keeping the generator inside of the capability area.

An example of a synchronous machine regulator model with a static exciter (usually a controlled thyristor rectifier) is shown in Figure 2.

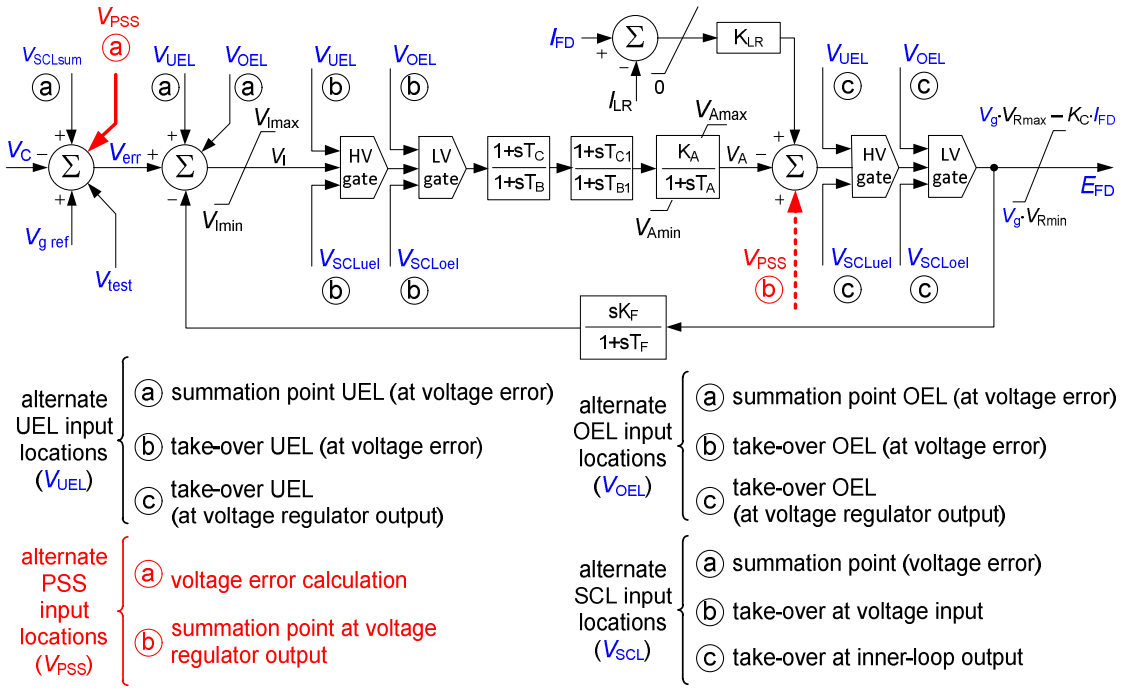

Figure 2. ST1C-type excitation system model [18].

Figure 2 shows the total gain of a static excitation system—gain K_A [18]. This gain includes the gain of the voltage regulation loop, the gain of the excitation transformer, and the gain of the thyristor firing card. A large K_A gain (i.e., K_A = 500) causes the excitation system to react strongly only to the voltage error. Unfortunately, this gain weakens the damping introduced by the damper windings and field windings. In the extreme case of a heavily loaded generator (and a long transmission line), a large K_A may result in net negative damping, thereby leading to an oscillatory a loss of stability [1]. On the other hand, a low value of K_A gain may trigger a loss of the system's voltage stability, which manifests itself in a voltage breakdown due to a small disturbance that is called the voltage collapse [25]. Therefore, in a synchronous machine regulator requires a PSS loop (Figure 1), which increases the damping of the local swing modes (0.7–3 Hz) and does not reduce damping of the inter-area modes (0–1 Hz). The alternate PSS input locations are shown in Figures 1 and 2.

3. Dual-Input PSS Theory

Several PSS models are currently applicable, but dual-input PSS-P-ω stabilizers (PSS2A, PSS2B, and PSS2C) have become the industry standard. With the above in mind, we will focus on dual-input stabilizers later in this paper. The input signals for the dual-input PSS are the generator active power and the compensated shaft speed deviation (both calculated from the Vg and Ig signals; Figure 1). The algorithm of the dual-input PSS-P-ω stabilizer is shown in Figure 3.

The PSS-P-ω principles can be explained by the swing equation (without damping) given by [26,27]:

$$2 \cdot H \cdot \Delta\omega = \int (\Delta P_m - \Delta P_g) dt \quad (1)$$

where H—inertia constant of turbine and synchronous generator, $\Delta\omega$—shaft speed deviation, P_m—mechanical power, and P_g—electrical power (generator active power).

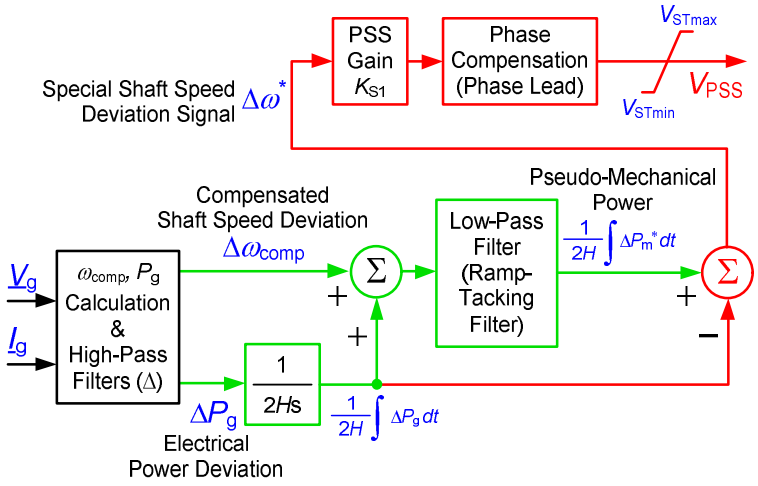

Figure 3. The algorithm of the dual-input PSS-P-ω stabilizer.

The green part of the PSS algorithm (Figure 3) is used to derive a signal proportional to the integral of the pseudo-mechanical power (P_m^*) deviation signal. This signal can be calculated using swing Equation (1) transformed into the following form:

$$\frac{1}{2H} \cdot \int \Delta P_m^* dt = \Delta\omega_{comp} + \frac{1}{2H} \cdot \int \Delta P_g dt \quad (2)$$

where $\Delta\omega_{comp}$—compensated shaft speed deviation calculated from the V_g and I_g signals (Figures 1 and 3) and a compensation reactance X_{COMP} [28] (where $X_{q'} < X_{COMP} < X_q$ [27]).

The relation (2) is used to calculate a signal by adding to compensated shaft-speed-deviation signal ($\Delta\omega_{comp}$) and the integral of the electrical power (P_g)-deviation signal. It would appear that nothing has been gained, but a subtle change was made. Generally, mechanical power deviations are quite slow relative to the shaft's mechanical oscillations, so a low-pass filter (Figure 3) derived the signal proportional to the integral of pseudo-mechanical power without slow variations in power.

The red part of the PSS algorithm (Figure 3) is used to derive a special shaft-speed-deviation signal (Δω*). This signal can be calculated using swing Equation (1) transformed into the following form:

$$\Delta\omega^* = \frac{1}{2H} \int \Delta P_m^* dt - \frac{1}{2H} \int \Delta P_g dt \quad (3)$$

The relation (3) is used to calculate a signal from the difference between the integral of the pseudo-mechanical power (P_m^*) deviation and the integral of the electrical power (P_g) deviation. This special shaft-speed-deviation signal (Δω* does not contain the unwanted run-out of the shaft and is referred to as the accelerating torque (or power because shaft speed changes are quite small)). The special shaft-speed-deviation signal is amplified in the PSS gain block (Figure 3) and then goes to the phase-compensation block.

4. PSS Parameter Selection

The settings of individual PSS parameters will be presented using the example of the PSS2C structure. The block diagram of the PSS2C is shown in Figure 4.

The sample values of all PSS2C settings can be found in the standard [18] in the form of Table 1.

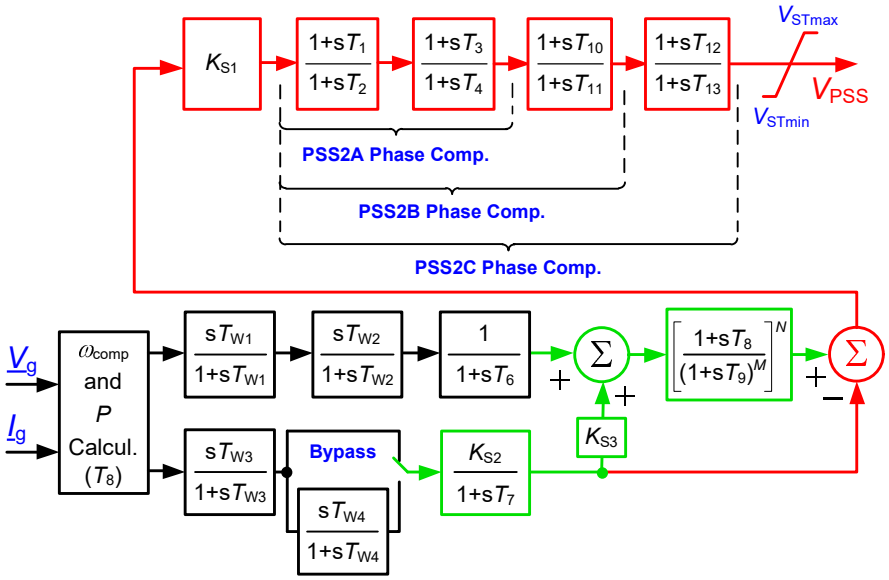

Figure 4. Block diagram of the PSS2C [18].

Table 1. Sample data (settings) for PSS2C stabilizer for ST1C model [18].

Description	Symbol	Type [e]	Value	Units
PSS gain	K_{S1}	A	20	pu
PSS gain	K_{S2}	E/A	[a]	pu
PSS gain	K_{S3}	E	1	pu
PSS transducer time constant	T_6	E	0.0	s
PSS transducer time constant [b]	T_7	A	10	s
PSS washout time constant	T_{W1}	A	10	s
PSS washout time constant	T_{W2}	A	10	s
PSS washout time constant	T_{W3}	A	10	s
PSS washout time constant	T_{W4}	A	[c]	s
PSS transducer time constant	T_8	A	0.30	s
PSS washout time constant	T_9	A	0.15	s
PSS low-pass filter exponent	M	A	2	-
PSS low-pass filter exponent	N	A	4	-
PSS numerator (lead, comp., 1st block)	T_1	A	0.16	s
PSS denominator (lag, comp., 1st block)	T_2	A	0.02	s
PSS numerator (lead, comp., 2nd block)	T_3	A	0.16	s
PSS denominator (lag, comp., 2nd block)	T_4	A	0.02	s
PSS numerator (lead, comp., 3rd block)	T_{10}	A	[d]	s
PSS denominator (lag, comp., 3rd block)	T_{11}	A	[d]	s
PSS numerator (lead, comp., 4th block)	T_{12}	A	[d]	s
PSS denominator (lag, comp., 4th block)	T_{13}	A	[d]	s
Maximum PSS output	V_{STmax}	A	0.20	pu
Minimum PSS output	V_{Stmin}	A	−0.066	pu

[a] The K_{S2} should be calculated as $T_7/2H$, where H is the generator inertia constant. [b] The time constant T_7 should be equal to T_{W2}. [c] The washout block with time constant T_{W4} should be bypassed. [d] The third and fourth lead-lag blocks were not used in this example. [e] Type A—adjustable parameter; Type E—equipment characteristic.

Almost all settings shown in Table 1 are marked as Type A, which means an adjustable parameter. However, by knowing the inertia constant H, we can calculate the values of T_7, K_{S2}, and T_8; and in most cases, we can use other PSS settings from Table 1 except for the following items, which require special selection (these settings are marked in red in the Table 1): phase compensation (T_1 T_2, T_3, T_4, T_{10}, T_{11}, T_{12}, and T_{13}) and PSS gain (K_{S1})—see Figure 4.

The settings of the phase compensation (Figures 3 and 4) are important because there is some delay between a field voltage change and the resulting magnetic-flux change inside the generator. Therefore, if the torque is to be injected in phase with the shaft speed change, it is necessary to "advance" the speed-change signal before applying it to the input of the exciter. A phase-compensation block achieves this function by shifting (leading) the special speed-signal deviation (Δω* in phase. This phase should compensate for the delay shift in the generator field circuit. The structure of the phase-compensation block of the PSS2C is shown in Figure 4.

The selection of the PSS2A phase compensation characteristic (Figure 4) is achieved by the selection of the values of the four time constants: T_1 T_2, T_3, and T_4. The phase-compensation block in the PSS2B is equipped with additional elements with the constants T_{10} and T_{11} and in the PSS3C with the constants T_{12} and T_{13}. So, the selection of the PSS2B phase-compensation characteristic requires the selection of six time constants and the selection of the PSS2C phase-compensation characteristic requires the selection of eight constants. An example of the PSS2A phase-compensation characteristics for three different values of T_1 and T_3 and a fixed value of T_2 and T_4 is shown in Figure 5 (see Section 5.5 and Figure 9; the best setting for that particular PSS was used: $T_2 = T_4 = 0.02$ s, $T_1 = T_3 = 0.20$ s).

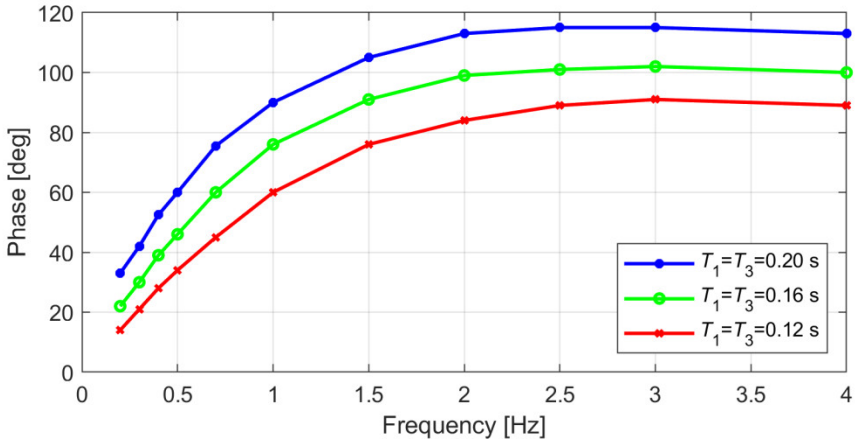

Figure 5. Examples of the PSS2A's phase-compensation characteristics (T_2 = T_4 = 0.02 s, T_1 = T_3 = 0.20 s/0.16 s/0.12 s).

The process of selecting the PSS gain K_{S1} is described in Section 5.4.

5. Overview of the PSS Tests Performed in the World

The PSS requirements specified by the transmission system operator (TSO) should also meet the requirements of the grid regulatory authority. The areas under the jurisdiction of several grid regulatory authorities and the areas of some of their TSOs are shown in Figure 6.

So, the requirements specified by the European TSOs should also meet the requirements of the European Union/European Network of Transmission System Operators for Electricity (EU/ENTSO-E). For example (as shown in Figure 6), the EU/ENTSO-E requirements specified in [29] should meet those of TSOs such as:

- NORDIC [30]—Denmark, Finland, Norway, Sweden;
- NGESO [31]—United Kingdom (UK);
- PSE [32]—Poland (PL).

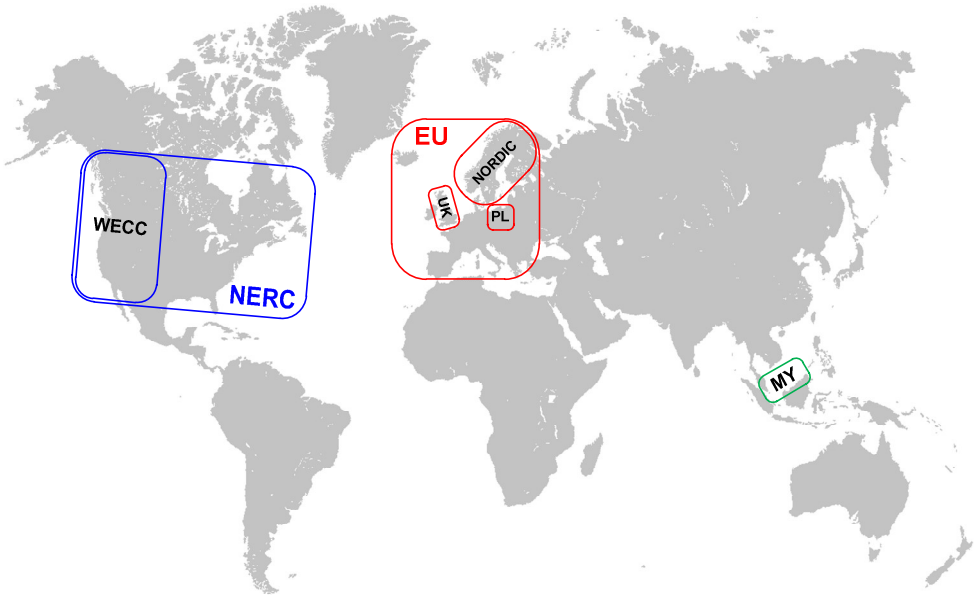

Figure 6. Areas under the jurisdiction of several grid regulatory authorities and some of their TSOs.

Similarly, the requirements specified by the North American TSOs such as the Western Electricity Coordinating Council (WECC) [33,34] should meet the requirements of the North American Electric Reliability Corporation (NERC) [28]. The situation is different in, for example, Malaysia (MY) [35–37], which does not have any overriding requirements (Figure 6). A summary of the PSS tests required by the above-mentioned grid regulatory authorities and tests required by their TSOs (Figure 6) is presented in Table 2.

Table 2. Summary of the PSS tests required (+) by grid regulatory authorities and their TSOs.

GRID REGULATORY AUTHORITY	NERC		EU, ENTSO-E				GCfPM
TSO / PSSTEST TYPE		WECC USA Canada Mexico		NORDIC Denmark Finland Norway Sweden	NGESO UK	PSE Poland	GCfPM Malaysia
PSS Simulation Studies	+	+	+	+	–	–	+
PSS Step-Response Test	+	+	–	–	+	–	+
PSS Damping Index Test	–	–	–	+	–	–	+
Frequency-Response Tests	+	+	–	+	+	–	+
PSS Gain-Margin Test	+	+	–	–	+	–	+
Line-Switching Test	–	–	–	–	–	–	+
PSS Limiting-Function Test	+	–	–	–	–	–	–
PSS/Limiter Interaction Test	–	+	–	–	–	–	–

The PSS tests presented in Table 2 will be described in detail in the following sections. The descriptions of the PSS tests are based on the current recommendations [28–38] and contain information on how to perform them and the acceptance criteria. Note that all PSS tests and simulations described below should be performed with the synchronous generator loaded to at least 0.8 pu of the full load (0.8 P_{gn}).

5.1. PSS Simulation Studies

PSS simulation studies should be performed carefully because there may be a difference between the performances of the input to the PSS, which may cause a difference in simulation vs. measurements (expert knowledge). This may be the case if the compensated shaft-speed-deviation signal is different than the shaft-speed deviation.

Acceptance Criteria [27]
"The simulation shall be deemed successful if the following conditions are cumulatively fulfilled: • the PSS function damps the existing active power oscillations of the power-generating module within a frequency range specified by the relevant TSO. That frequency range shall include the local mode frequencies of the power-generating module and the expected network oscillations, • a sudden load reduction of the power-generating module from 1 to 0.6 pu of the maximum capacity does not lead to undamped oscillations in active or reactive power of the power-generating module."

5.2. PSS Step-Response Test

The step-response test shall be performed by injecting a step signal (0.02–0.03 pu) into the automatic voltage regulator reference $V_{\text{g ref}}$ (Figures 1 and 2).

Acceptance Criteria
The test should demonstrate a greater damping of the active power oscillations with a PSS compared to the oscillations without a PSS (Figure 7).

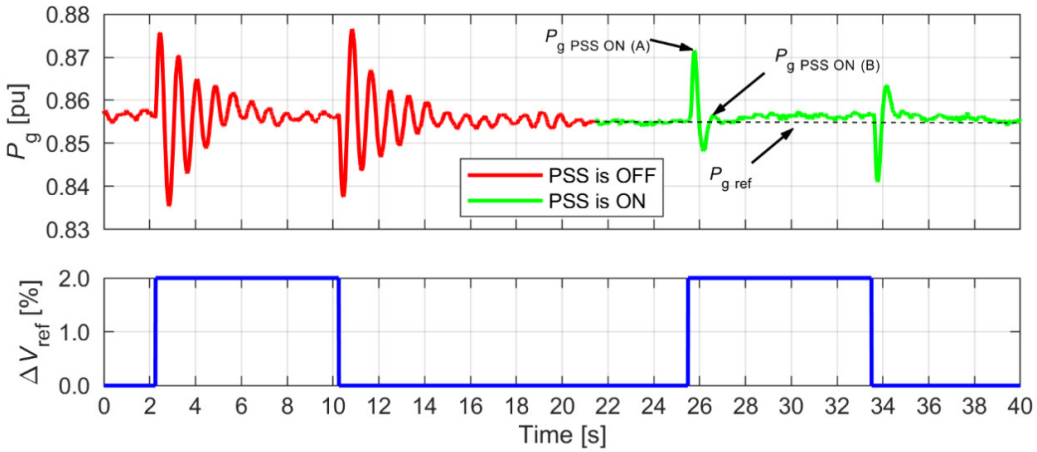

Figure 7. PSS step-response test with PSS OFF and PSS ON [39].

5.3. PSS Damping Measurement from Step-Response Test

The PSS step-response test (described above) can be used to calculate the damping value of the power oscillations with a PSS compared to the active power oscillations without a PSS. This damping (damping index DR) is calculated from the ratio of the two active power overshoots ($P_{\text{g PSS ON}}$ (A), $P_{\text{g PSS ON}}$ (B); see Figure 7). The damping index DR is given by:

$$DR = \frac{\delta}{\sqrt{4\pi^2 + \delta^2}} \tag{4}$$

where the logarithmic decrement is:

$$\delta = \ln\left(\frac{P_{\text{g PSS ON }(A)} - P_{\text{g ref}}}{P_{\text{g PSS ON }(B)} - P_{\text{g ref}}}\right) \tag{5}$$

Acceptance Criteria
The test should demonstrate a greater damping of the active power oscillations with a PSS compared to the damping of the active power oscillations without a PSS (Figure 7), and the damping index DR (4) shall be greater than X% (where the X value is given by the TSO).

5.4. PSS Gain Test

The selection of the PSS gain K_{S1} (Figures 3 and 4) should be adjusted during commissioning. The PSS gain margin (K_{S1_LIM}) is identified by slowly increasing the PSS gain until a rapid active power oscillation occurs (when $K_{S1} = K_{S1\_LIM}$). For good stability of the control loop, the PSS gain K_{S1} should be reduced to $1/3 \cdot K_{S1\_LIM}$ [1,34].

Before the PSS gain test, the K_{S1} should be increased twice ($2 \cdot K_{S1}$). With this temporary increased gain, the step-response test (see Section 5.2) should be done. After this test, the PSS gain should of course be restored to its original value (K_{S1}).

Acceptance Criteria
No active power oscillations should occur during the step-response test with the PSS gain increased twice ($2 \cdot K_{S1}$).

5.5. PSS Frequency-Response Tests

The PSS frequency-response tests with and without a PSS shall be performed by one of the following methods (V_{test} is shown in Figures 1 and 2):

- Injecting a sequence of sinusoidal V_{test} signals in the range of 0.1–5 Hz at an interval of 0.1 Hz,
- Injecting white noise as a V_{test} signal and using fast Fourier transform,
- Generating an impulse (impulse test) of a V_{test} signal and using fast Fourier transform; this test is typically larger in magnitude than the PSS step-response test (0.10 pu vs. 0.02 pu) but for much shorter durations (0.1–0.5) s.

Based on the tests with and without a PSS, we could achieve a comparison of the active power frequency response with PSS—$G_{PSS\ ON}(f)$ vs. the active power frequency response without PSS—$G_{PSS\ OFF}(f)$. The active power frequency response without a PSS will indicate the frequency of the local mode oscillation. However, this will not indicate the inter-area oscillations because they are very difficult to excite with a single generator connected to the grid. In addition, the test without a PSS can achieve the characteristic of the phase between the terminal voltage and the injected V_{test} signal. This characteristic can be used (in the case of PSS2A, PSS2B, or PSS2C) to verify the PSS's phase-compensation settings through selection of the time constants (Figure 5).

Acceptance Criteria
The active power frequency-response test shall demonstrate damping of the active power frequency response with a PSS compared to the active power frequency response without a PSS (Figure 8). In the case of a dual-input PSS-P-ω stabilizer, the sum of the PSS's phase-compensation characteristic and the phase characteristic of the generator terminal voltage (V_g, Figure 1) without a PSS must be close to 0 degrees in the inter-area modes (0–1 Hz). If local stability concerns require PSS settings that result in an inter-area phase shift other than zero, the settings should not result in a phase shift over −30 degrees in the inter-area modes (Figure 9).

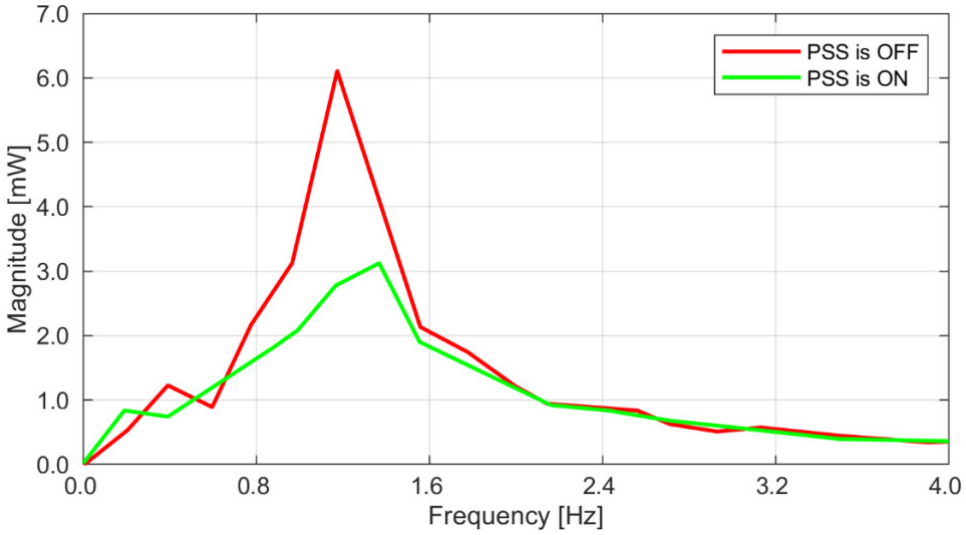

Figure 8. Impulse test fast Fourier transform [28].

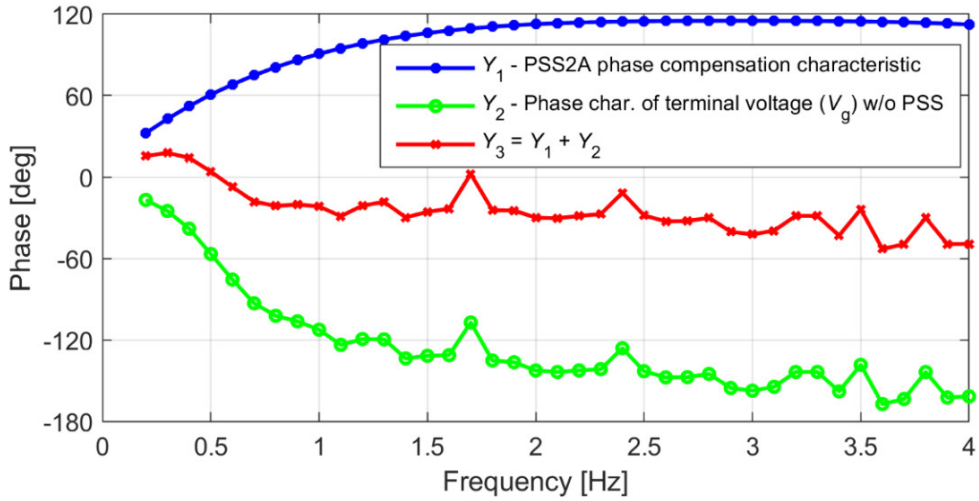

Figure 9. PSS phase characteristics [40] (phase compensation: $T_2 = T_4 = 0.02$ s, $T_1 = T_3 = 0.20$ s).

5.6. Line-Switching Test

The line-switching test with and without a PSS shall be performed by using a line-switching operation or changing the tap of the generator's step-up transformer.

Acceptance Criteria
The test should demonstrate a greater damping of the active power (less oscillation) with a PSS compared to the damping of the active power oscillations without a PSS during the same tap change (i.e., from tap 10 to 11, as shown in Figure 10).

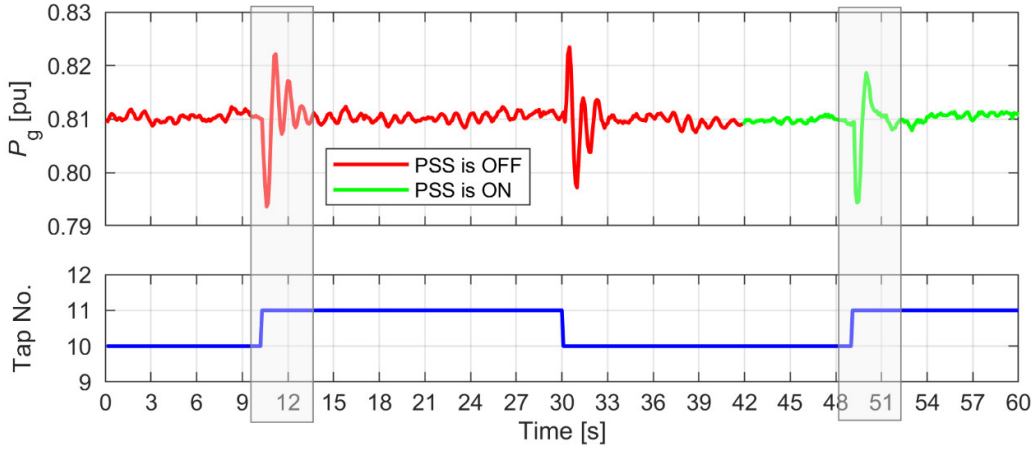

Figure 10. Changing the tap of the step-up transformer [40].

5.7. PSS Limiting-Function Test

The PSS limiting-function test shall be performed by increasing the input signal or increasing the PSS gain until the PSS output signal is clipped. The settings of the PSS limiting function (V_{STmax}, V_{STmin}) are presented in Table 1.

Acceptance Criteria
Verification can be carried out by measuring the PSS output signal (V_{PSS} in Figures 1–4). The PSS output signal cannot move the generator terminal voltage beyond a preset setting. A typical range of V_{STmax} and V_{STmin} settings is from ±5% to ±10% of the rated generator terminal voltage. Moreover, the asymmetrical limits may be employed.

5.8. PSS/Limiter Interaction Test

All limiters of the synchronous machine regulator (Figure 1; alternate limiter inputs are shown in Figure 2) must be coordinated with the PSS to ensure a stable performance during limiter operation. For example, after the PSS gain is set, the machine should remain underexcited until the under-excitation limiter (UEL) becomes active. Then the step-response test (see Section 5.2) should be conducted, and no active power oscillations should occur.

Acceptance Criteria
The test should demonstrate that there is no interaction or instability between the PSS and each limiter.

5.9. Summary of the PSS Tests

In the above PSS tests, there was only one performance index that described the quality of the PSS as a value—the damping index DR (see Section 5.3). In our opinion, it is necessary to define additional performance indices that describe the quality of a PSS as values.

Such new indices would be particularly useful in relation to the active power frequency response with a PSS and the active power frequency response without a PSS. Currently, the relationship between these responses (acceptance criteria) is given in Description (1) below.

Description (1)—Relation of the active power-frequency response with and without a PSS
The frequency range of the inter-area oscillations (0.15–0.6 Hz) characteristic of a PSS should indicate the same or better damping than without the PSS (see Figure 12). Additionally, the range of local-area oscillations (1.0–2.0 Hz) characteristic of the PSS should indicate better damping than without the PSS. In other words, the characteristic with the PSS should not lie above the characteristic without the PSS. For frequencies higher than 2 Hz, the characteristic with the PSS may lie above the one without the PSS, but the differences between these characteristics should not be large.

The process of replacing the above Description (1) with new indices is described in the next part of this paper. These new indices must of course be defined together with the new acceptance criteria.

6. New PSS Performance Indices

Figure 11 contains an example of $G_{\text{PSS OFF}}(f)$—the active power frequency response without PSS—showing the characteristic of the active power oscillation amplitude vs. the V_{test} signal amplitude. The maximum frequency of the response should allow viewing of the entire "resonance" part of the $G_{\text{PSS OFF}}(f)$ characteristic (around 1.6 Hz in Figure 11). This makes it necessary to measure the "resonant frequency" at least twice. The exact method of measuring this characteristic is described in Section 5.5.

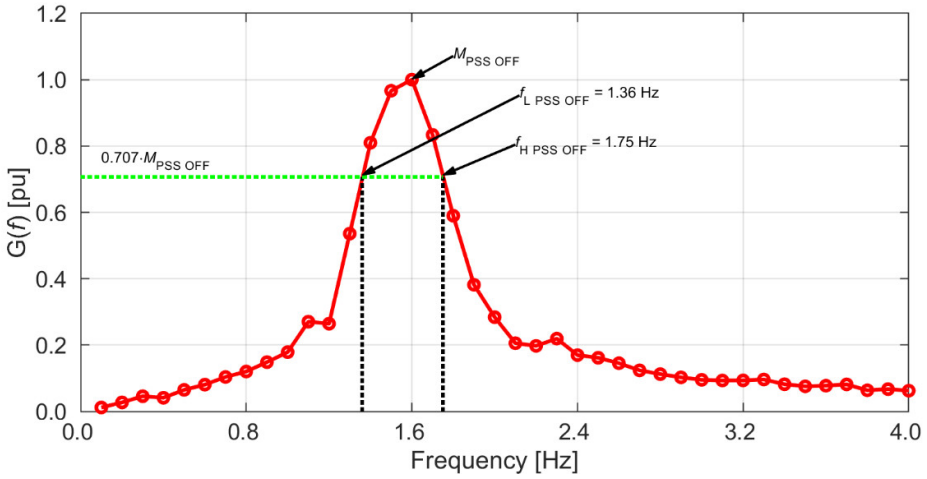

Figure 11. Active power frequency response $G_{\text{PSS OFF}}(f)$, test conditions: PSS is OFF, P_g = 382 MW, Q_g = 0 Mvar [39].

It is important to note that for all of the frequency responses listed below (Figures 11–18), the vertical axis was scaled so that the maximum of the characteristic $G_{\text{PSS OFF}}(f)$ (without PSS) was equal 1.0 pu.

The maximum of the active power frequency response without a PSS (Figure 11) is given by:

$$M_{\text{PSS OFF}} = \max_f |G_{\text{PSS OFF}}(f)| \tag{6}$$

The shape of the active power frequency response without a PSS (Figure 11) is similar to the frequency response of the bandpass filter. Therefore, the active power frequency response without a PSS can be described using the same parameters as the bandpass filter [38] such as:

- $f_{\text{L PSS OFF}}$—Lower cutoff frequency for which the active power frequency response $G_{\text{PSS OFF}}(f)$ becomes greater than −3 dB level, which means the level 0.707 $M_{\text{PSS OFF}}$ (6),
- $f_{\text{H PSS OFF}}$—Upper cutoff frequency for which the active power frequency response $G_{\text{PSS OFF}}(f)$ becomes smaller than −3 dB level, which means level 0.707 $M_{\text{PSS OFF}}$ (6),

- $f_{0\ \mathrm{PSS\ OFF}}$—Center frequency, which is a measure of a central frequency between the upper and lower cutoff frequencies and is defined as the geometric mean of these frequencies:

$$f_{0\ \mathrm{PSS\ OFF}} = \sqrt{f_{\mathrm{L\ PSS\ OFF}} \cdot f_{\mathrm{H\ PSS\ OFF}}} \tag{7}$$

Based on the $G_{\mathrm{PSS\ OFF}}(f)$ characteristic (Figure 11) and according to the above considerations and relations (6) and (7), the following parameters were determined:

- $M_{\mathrm{PSS\ OFF}}$ = 1.00;
- $f_{\mathrm{L\ PSS\ OFF}}$ = 1.36 Hz;
- $f_{\mathrm{H\ PSS\ OFF}}$ = 1.75 Hz;
- $f_{0\ \mathrm{PSS\ OFF}}$ = 1.54 Hz.

Figure 12 shows the active power frequency response without a PSS (copied from Figure 11) and the active power frequency response with PSS (PSS is ON)—$G_{\mathrm{PSS\ ON}}(f)$ (see Section 5.5).

Similar to relation (6), the maximum of the active power frequency response with the PSS (Figure 12, PSS is ON) is given by:

$$M_{\mathrm{PSS\ ON}} = \max_{f} |G_{\mathrm{PSS\ ON}}(f)| \tag{8}$$

The $G_{\mathrm{PSS\ ON}}(f)$ characteristic (Figure 12; PSS is ON) may be described using parameters similar to $G_{\mathrm{PSS\ OFF}}(f)$ such as the lower cutoff frequency, upper cutoff frequency, and center frequency. The last parameter is given by:

$$f_{0\ \mathrm{PSS\ ON}} = \sqrt{f_{\mathrm{L\ PSS\ ON}} \cdot f_{\mathrm{H\ PSS\ ON}}} \tag{9}$$

Based on the $G_{\mathrm{PSS\ ON}}(f)$ characteristic (Figure 12; PSS is ON) and according to the above considerations and relations (8) and (9), the following parameters were determined:

- $M_{\mathrm{PSS\_ON}}$ = 0.39;
- $f_{\mathrm{L\ PSS\ ON}}$ = 1.40 Hz;
- $f_{\mathrm{H\ PSS\ ON}}$ = 1.92 Hz;
- $f_{0\ \mathrm{PSS\ ON}}$ = 1.64 Hz.

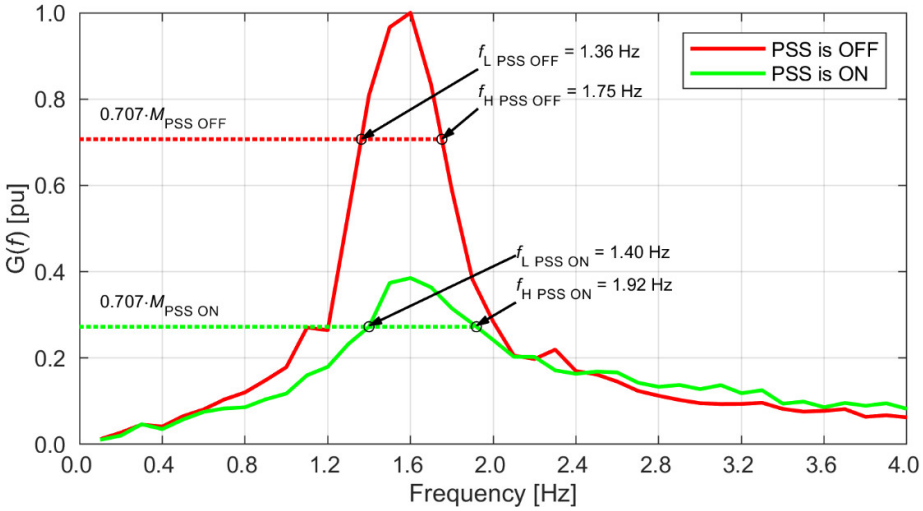

Figure 12. Active power-frequency responses $G_{\mathrm{PSS\ OFF}}(f)$ and $G_{\mathrm{PSS\ ON}}(f)$ under the following test conditions: PSS is OFF/ON, P_g = 382 MW, Q_g = 0 Mvar [39].

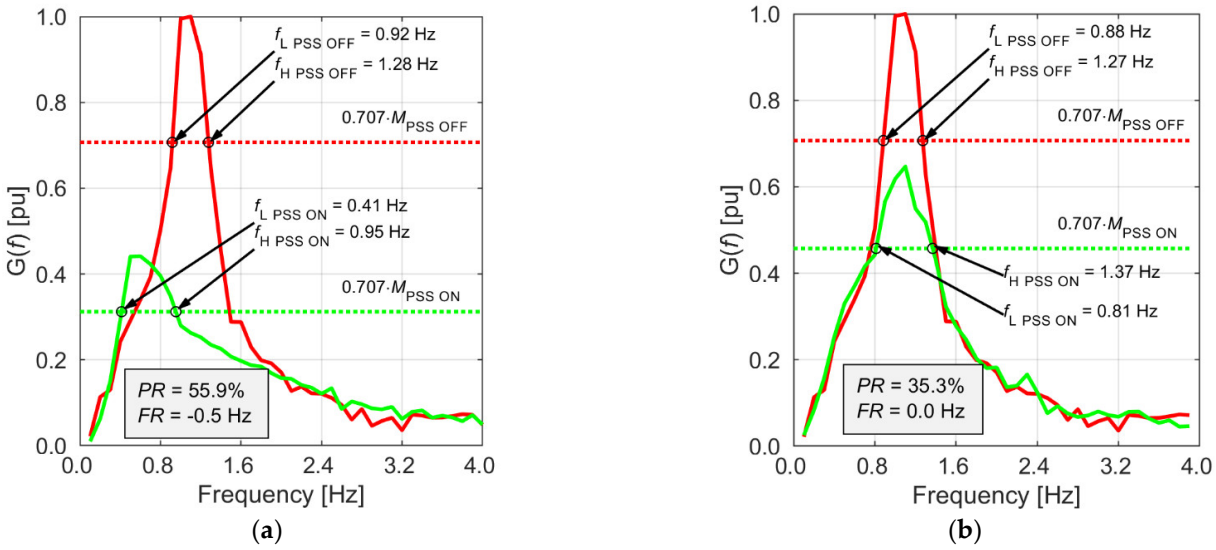

Figure 13. $G_{PSS\ OFF}(f)$ and $G_{PSS\ ON}(f)$ for two sets of the PSS settings (**a**,**b**) under the following test conditions: PSS is OFF/ON, P_g = 140 MW, Q_g = 0 Mvar [40].

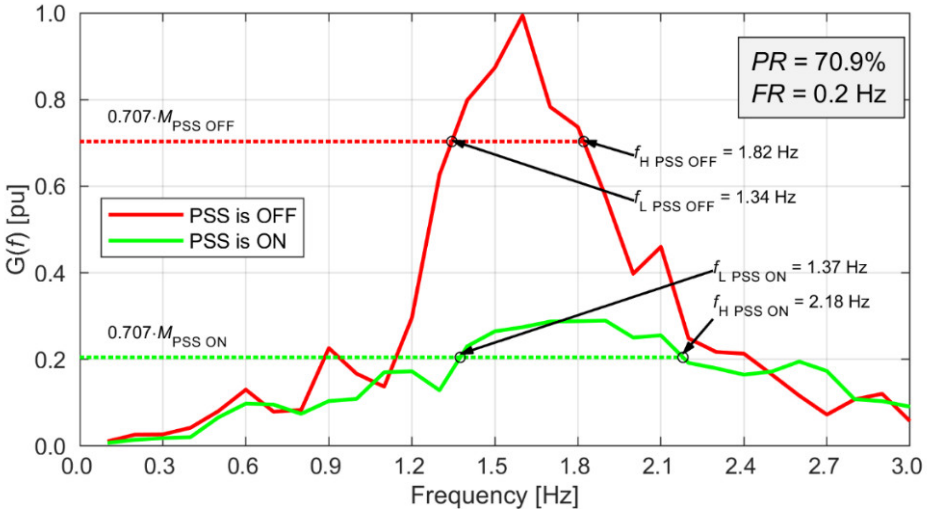

Figure 14. $G_{PSS\ OFF}(f)$ and $G_{PSS\ ON}(f)$, P_g = 370 MW, Q_g = 5 Mvar [41].

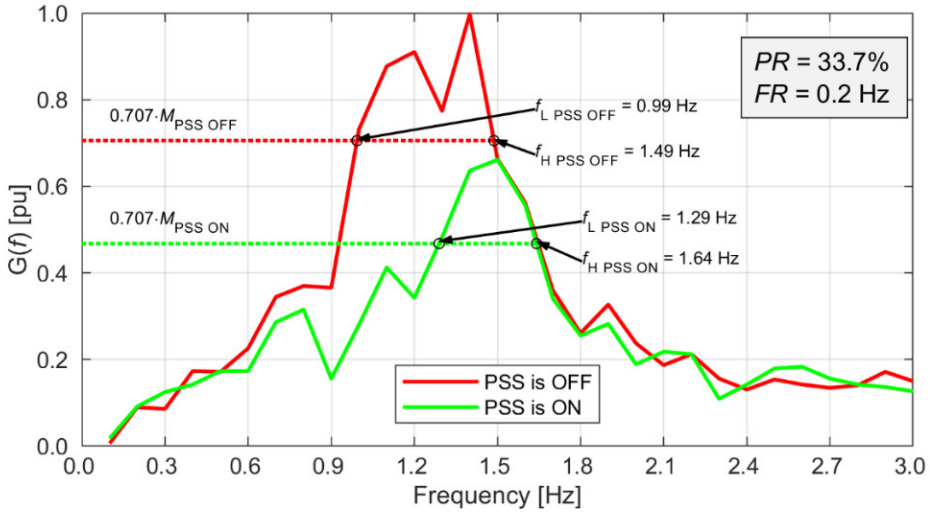

Figure 15. $G_{PSS\ OFF}(f)$ and $G_{PSS\ ON}(f)$, P_g = 140 MW, Q_g = 0 Mvar [42].

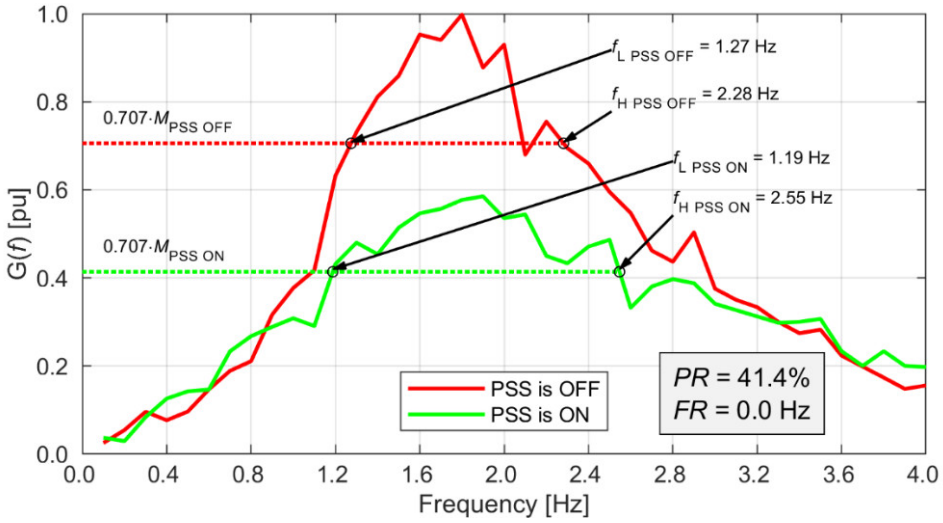

Figure 16. $G_{\mathrm{PSS\ OFF}}(f)$ and $G_{\mathrm{PSS\ ON}}(f)$, P_g = 400 MW, Q_g = 4 Mvar [43].

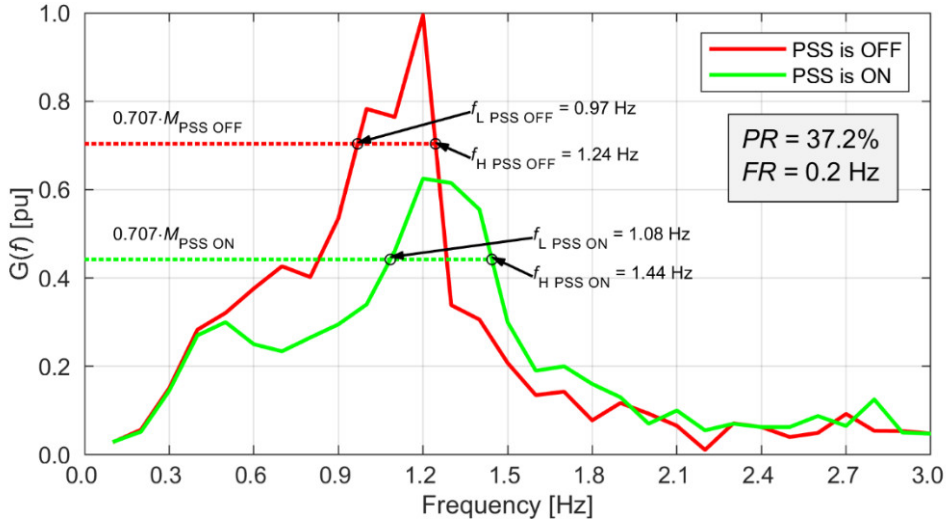

Figure 17. $G_{\mathrm{PSS\ OFF}}(f)$ and $G_{\mathrm{PSS\ ON}}(f)$, P_g = 208 MW, Q_g = 0 Mvar [44].

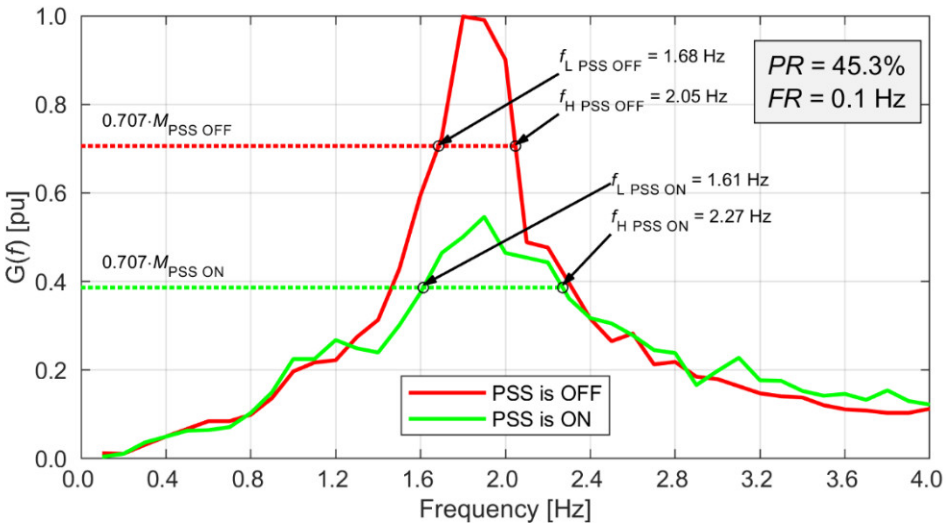

Figure 18. $G_{\mathrm{PSS\ OFF}}(f)$ and $G_{\mathrm{PSS\ ON}}(f)$, P_g = 600 MW, Q_g = 0 Mvar [45].

The authors' experience [39–45] shows that the active power-frequency responses of PSSs typically have one dominant "resonance frequency"—the local mode frequency (see Figures 14–18), which is similar to the bandpass filter. Therefore, for the evaluation of the PSS damping, a suitable index seems to be the difference between value 1 and the ratio of the $M_{\text{PSS ON}}$ (8) and $M_{\text{PSS OFF}}$ (6) in percent. This first index, which will be called the peak ratio (*PR*), is given by the relation:

$$PR = \left(1 - \frac{M_{\text{PSS ON}}}{M_{\text{PSS OFF}}}\right) \cdot 100\% = \left(1 - \frac{\max\limits_{f} |G_{\text{PSS ON}}(f)|}{\max\limits_{f} |G_{\text{PSS OFF}}(f)|}\right) \cdot 100\% \tag{10}$$

To check the properties of the *PR* index, we considered the characteristics shown in Figure 13 that were measured during the commissioning of PSS2B [40]. *PR* indices calculated according to relation (10) are shown in Figure 13; both indices had values greater than 0% (characteristic in Figure 13a has *PR* = 55.9% and characteristic in Figure 13b has *PR* = 35.3%), therefore both characteristics showed proper damping introduced by the PSS. Moreover, the *PR* index in Figure 13a is greater than *PR* index in Figure 13b, so:

- The characteristic in Figure 13a shows higher damping,
- The characteristic in Figure 13b shows lower damping.

However, if we look at the characteristics from the point of view of the acceptance criteria given in Description (1) (see Section 5.9):

- The characteristic in Figure 13a did not meet the acceptance criteria given in the description,
- The characteristic in Figure 13b met the acceptance criteria given in the description.

Bearing the above in mind, an additional index is necessary to verify the properties of the PSS characteristics.

To verify the correctness of the PSS tuning using the active power-frequency response, we propose a second index. For the evaluation of the PSS damping, a suitable index seems to be the difference between $f_{0\_PSS\_ON}$ (9) and $f_{0\_PSS\_OFF}$ (7). This second index will be called the frequency ratio (*FR*) and is given by the relation:

$$FR = f_{0\ \text{PSS ON}} - f_{0\ \text{PSS OFF}} = \sqrt{f_{\text{L PSS ON}} \cdot f_{\text{H PSS ON}}} - \sqrt{f_{\text{L PSS OFF}} \cdot f_{\text{H PSS OFF}}} \tag{11}$$

So, if the value of *FR* (11) is less than 0 Hz then the center frequency of the characteristic with PSS (9) is shifted from the center frequency of the characteristic without PSS (7) to a lower frequency (Figure 13a). If the value of *FR* is equal to 0 Hz then the center frequencies of characteristics (with and without PSS; Figure 13b) are equal. If the value of FR is greater than 0 Hz then the center frequency of the characteristic with PSS (9) is shifted from the center frequency of the characteristic without PSS (7) to a higher frequency.

FR indices calculated according to relation (11) are shown in Figure 13. The characteristic in Figure 13a has *FR* = −0.5 Hz, and the characteristic in Figure 13b has *FR* = 0.0 Hz.

Therefore, despite the high damping shown in Figure 13a (*PR* = 55.9%), the shift of the center frequency of this characteristic to lower frequencies (*FR* = −0.5 Hz) proved the low effectiveness of the PSS and did not meet the acceptance criteria (given in Description (1); see Section 5.9). The characteristic in Figure 13b has a lower damping (*PR* = 35.3%) but did not shift the center frequency of the characteristic with the PSS (*FR* = 0.0 Hz) and met the acceptance criteria (given in the description). However, the active power-frequency response's characteristic with *FR* = 0 Hz was a borderline case (Figure 13b). The PSS will have better properties if the frequency range corresponding to the inter-area modes (0–1) Hz introduces greater damping. The fulfilment of this requirement will be ensured by the shift of the center frequency of the characteristic with a PSS to higher frequencies. Thus, $FR \geq 0$ Hz and $PR > 0$ is the desired effect. Operation of the proposed indices (*PR* and *FR*) will be verified by the active power frequency-response characteristics of the several

different synchronous generators shown in Figures 14–18. The characteristics came from the commissioning of the PSSs we carried out on real objects [39–45].

The values for *PR* and *FR* of the active power frequency-response characteristics of the several synchronous generators shown in Figures 12, 13b and 14–18 are presented in Table 3.

Table 3. Summary of *PR* and *FR* indices of the dual-input stabilizer (PSS-P-ω) characteristics.

PSS No	Figure	Src	S_n (MVA)	Location	PSS Type	Exciter Type	$f_{0\ PSS\ OFF}$ (Hz)	$f_{0\ PSS\ ON}$ (Hz)	*PR*(%)	*FR*(Hz)
1	Figure 12	[39]	426	PL	PSS2A	STATIC	1.54	1.64	39.0	0.1
2	Figure 13b	[40]	210	MY	PSS2B	ROTAT.	1.06	1.05	35.3	0.0
3	Figure 14	[41]	459	PL	PSS2A	STATIC	1.56	1.73	70.9	0.2
4	Figure 15	[42]	209	PL	PSS2A	STATIC	1.21	1.45	33.7	0.2
5	Figure 16	[43]	472	USA, AZ	PSS2A	STATIC	1.70	1.74	41.4	0.0
6	Figure 17	[44]	271	PL	PSS2A	ROTAT.	1.10	1.25	37.2	0.2
7	Figure 18	[45]	902	USA, IA	PSS2A	STATIC	1.86	1.91	45.3	0.1

The active power frequency-response characteristics presented in Figures 12, 13b and 14–18 met the acceptance criteria given in Description (1) (see Section 5.9). At the same time, these characteristics had *PR* indices (10) greater than 33% (Table 3) and *FR* indices (11) greater than or equal to 0 Hz (Table 3). This fact confirmed that the PSS had the correct properties (i.e., the PSS was fine-tuned) if the active power frequency-response characteristic met the following system of inequalities:

$$\begin{cases} PR > 0 \\ FR \geq 0 \end{cases} \tag{12}$$

The *FR* index as described by relation (11) can be presented in a graphical form (3D diagram) as a function of the frequencies $f_{0\ PSS\ ON}$ and $f_{0\ PSS\ OFF}$ described by the relations (6) and (8). A 3D view of the *FR* index (general relation) on the $f_{0\ PSS\ OFF}$–$f_{0\ PSS\ ON}$ plane for both frequencies in the range of 1 Hz to 2 Hz is shown in Figure 19.

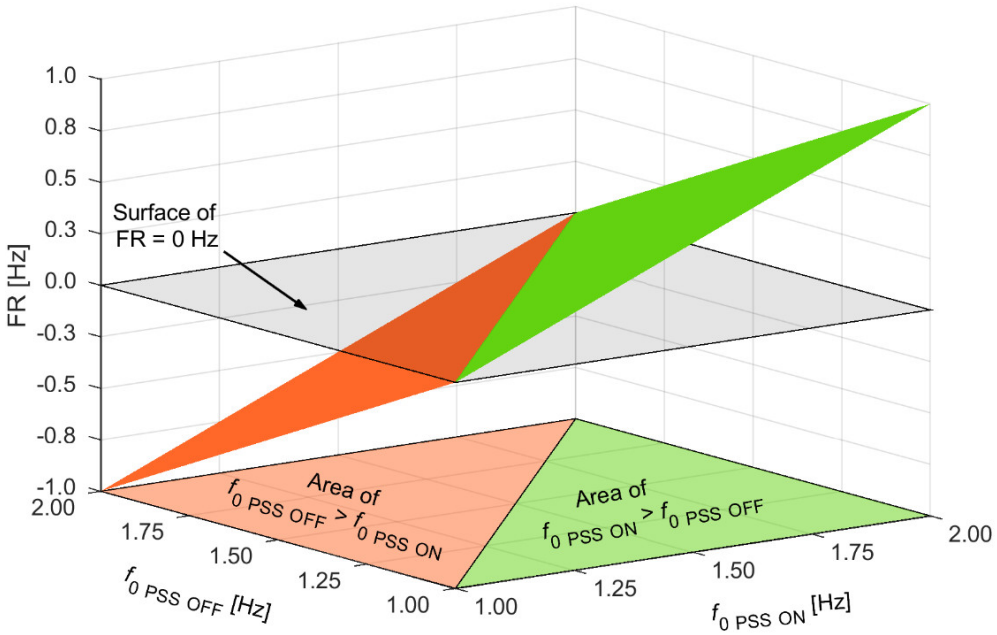

Figure 19. 3D graphical presentation of the *FR* index plotted on the $f_{0\ PSS\ ON}$-$f_{0\ PSS\ OFF}$ plane (general relation).

FR indices that meet the system of inequalities (12) must be located on the $f_{0\ \mathrm{PSS\ ON}}$–$f_{0\ \mathrm{PSS\ OFF}}$ plane in the triangular area of $f_{0\ \mathrm{PSS\ ON}} > f_{0\ \mathrm{PSS\ OFF}}$ or on its border $FR = 0$ (Figure 19; green triangle and border between green and red). According to the system of inequalities (12), the *PR* indices of the fine-tuned power system stabilizers ($PR > 0$) should be located on the $f_{0\ \mathrm{PSS\ OFF}}$–$f_{0\ \mathrm{PSS\ ON}}$ plane in the above-mentioned area. In order to verify this idea, the *PR* indices of the PSS2A and PSS2B from Table 3 are shown in Figure 20 in the form of pyramids on the $f_{0\ \mathrm{PSS\ OFF}}$–$f_{0\ \mathrm{PSS\ ON}}$ plane.

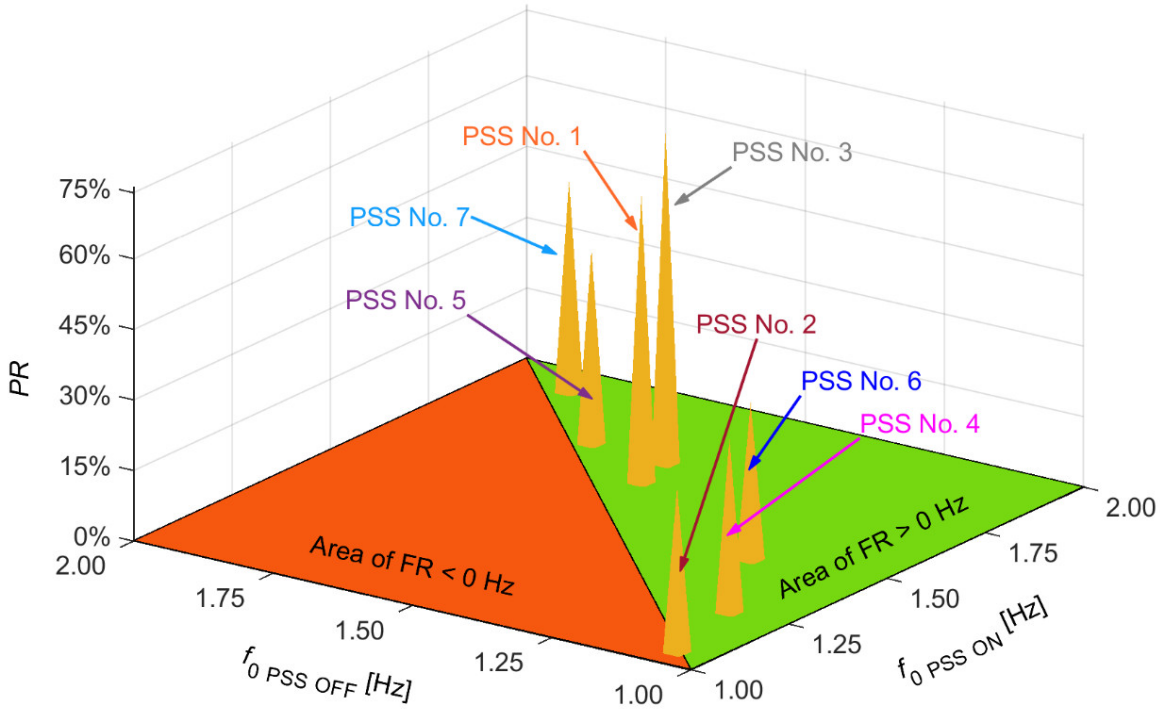

Figure 20. A 3D presentation of the *PR* indices from Table 3 plotted on the $f_{0\ \mathrm{PSS\ ON}}$–$f_{0\ \mathrm{PSS\ OFF}}$ plane.

All pyramids (*PR* indices) in Figure 20 "stick out" above the horizontal surface of $PR = 0\%$. Moreover, all pyramids stand in the area of $f_{0\ \mathrm{PSS\ ON}} > f_{0\ \mathrm{PSS\ OFF}}$ or on its border $FR = 0$. The 3D graphical presentation of the *PR* indices confirmed that all seven active power frequency response characteristics met the system of inequalities (12).

Based on the presented examples, we concluded that the active power frequency-response characteristics met the acceptance criteria given in Description (1) (see Section 5.9) if they met the system of inequalities (12).

The 3D diagram (Figure 20) enabled quick verification and comparison of the settings quality of the many PSSs. In particular, if we took into account the similar generating units connected to the same node of the transmission system, the detection of incorrect PSS settings was immediate. The benefits of these new indicators were best seen when the characteristics of $G_{\mathrm{PSS\ ON}}(f)$ and $G_{\mathrm{PSS\ OFF}}(f)$ were combined into one graph (Figure 21). Such a comparison then became very difficult in contrast to the same PSS characteristics presented by the new PSS indices in Figure 20.

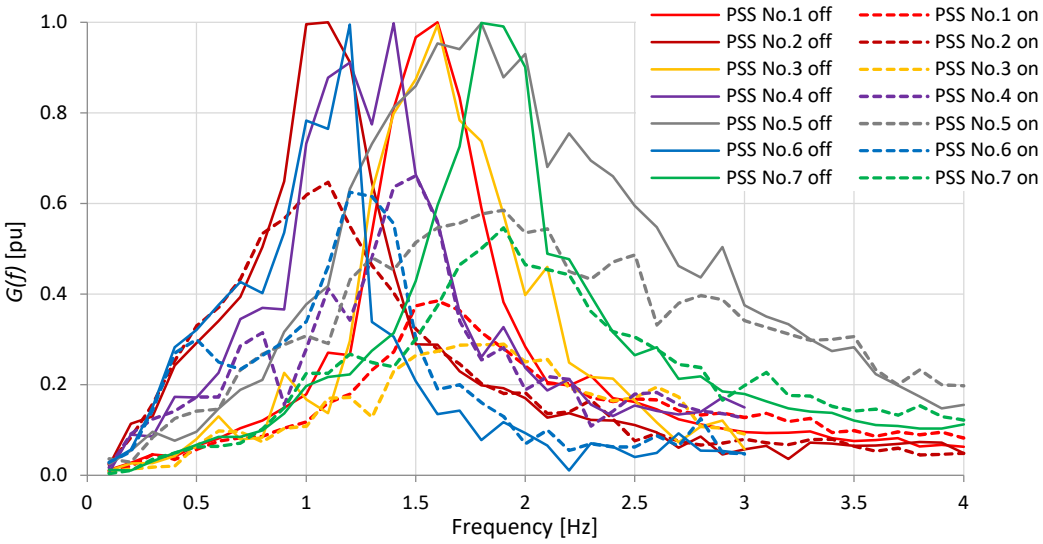

Figure 21. Active power frequency-response characteristics from Figures 12, 13b and 14–18.

7. Discussion

The summary of the required PSS tests presented in this paper in Table 2 showed that these tests were different in different power systems. Moreover, these tests were different for transmission system operators (TSOs) even though they worked in the same large power system. We recommend standardizing the list of the required PSS tests according to Table 2. The part of these tests that should be required by all TSOs is the PSS frequency-response test (active power frequency-response test) that was discussed in more detail in Section 5.5. The new proposed indices of the PSS were based on the active power frequency-response characteristic with a PSS and without a PSS. The measurement of these indices (the peak ratio *PR* (10) and the frequency ratio *FR* (11)) should be required as a part of an acceptance test of a synchronous machine regulator. The acceptance criteria for these indices should be the system of inequalities (12).

The value of the *PR* index is strongly connected to the PSS gain K_{S1} (see Section 5.4), which is limited to no more than 1/3 of its critical gain K_{S1_LIM} [1,33]. To solve this problem and provide enough damping in the inter-area modes, a parallel block added to the conventional PSS can be used [8], but in this case, the excitation system model will not conform to the standard [18]. The *PR* indices in Table 3 had values greater than 33%, so doubts may be raised by the weak criterion of $PR > 0$ (12). However, it was not possible to tighten the *PR* index criterion due to the PSS quality assessment method—the relative damping test. Only a detailed analysis of the absolute value of the active power damping would show how much the PSS function could increase the damping of active power oscillations.

The correlation between the *PR* indices of a large number of power system stabilizers (shown in Figure 20—3D graph) and the power system stability can be also the subject of further analysis. The analysis of the correlation between the *PR* indices may be the topic of a future article; the 3D graph of the *PR* indices can be used to compare the PSSs features before and after optimization.

The comparative analysis of the active power frequency-response characteristics with a PSS and without a PSS (shown in Figure 21) was very difficult, but when using new indices and the 3D diagram (Figure 20), it was efficient and effective. Moreover, the 3D graph solved the issue of whether the PSS provided (with accuracies specified by the authors of $PR > 0$ and $FR \geq 0$) sufficiently good damping properties of the active power oscillation in the frequency domain and in the time domain.

8. Conclusions

This paper presented two new performance indices for the PSS (peak ratio—*PR* and frequency ratio—*FR*), the methods of determining both indices, as well as how to apply them in practice, which was demonstrated by the tests of the real synchronous generators in the power system. Based on the obtained measurement results, recommended values of new indices were indicated. Due to their simplicity, the new performance indices proposed in this paper have great potential for practical application.

The new indices allow for the effective finding of PSSs with incorrect settings and (as a result after adjusting the PSS settings) to improve the stability of the power system, thus mitigating the risk of power system collapse.

The implementation of the proposed new indices by the TSO (which would require changing the current recommendations) will allow for a quick diagnosis of the condition of the analyzed fragment of the power system via the graphical visualization of the properties of many synchronous generators equipped with PSSs in a single 3D diagram. This article showed that a comparative analysis of PSS active power frequency-response characteristics was very difficult and laborious, but using the proposed new PSS indices and the 3D diagram allowed us to clearly present the effectiveness of the tested PSSs. As a result, it enabled the quick and effective identification of generating units that did not provide sufficient damping of the active power oscillations.

Author Contributions: Conceptualization, M.I.; methodology, M.I.; software, M.I.; validation, M.I.; formal analysis, M.I., R.M. and P.M.; investigation, M.I.; resources, M.I.; data curation, M.I.; writing—original draft preparation, M.I.; writing—review and editing, R.M. and P.M; supervision, R.M. and P.M.; All authors have read and agreed to the published version of the manuscript.

Funding: This research received no external funding.

Data Availability Statement: Not applicable.

Conflicts of Interest: The authors declare no conflict of interest.

References

1. Machowski, J.; Lubosny, Z.; Bialek, J.; Bumby, J.R. *Power System Dynamics. Stability and Control*; John Wiley & Sons: Hoboken, NJ, USA, 2020; ISBN 9781119526346.
2. Kundur, P. *Power System Stability and Control*; McGraw-Hill Education: New York, NY, USA, 1994; ISBN 9780070359581.
3. Tuttokmagi, O.; Kaygusuz, A. Transient Stability Analysis of a Power System with Distributed Generation Penetration. In Proceedings of the 7th International Istanbul Smart Grids and Cities Congress and Fair (ICSG), Istanbul, Turkey, 25–26 April 2019; pp. 154–158.
4. You, S.; Kou, G.; Liu, Y.; Zhang, X.; Cui, Y.; Till, M.J.; Yao, W. Impact of High PV Penetration on the Inter-Area Oscillations in the U.S. Eastern Interconnection. *IEEE Access* **2017**, *5*, 4361–4369. [CrossRef]
5. Orosz, T.; Rassolkin, A.; Kallaste, A.; Arsenio, P.; Panek, D.; Kaska, J.; Karban, P. Robust design optimization and emerging technologies for electrical machines: Challenges and open problems. *Appl. Sci.* **2020**, *10*, 6653. [CrossRef]
6. Paszek, S.; Nocoń, A. *Optimisation and Polyoptimisation of Power System Stabilizer Parameters*; LAP LAMBERT Academic Publishing: Lambert, Saarbrucken, 2014.
7. Paszek, S.; Nocoń, A. Parameter polyoptimization of PSS2A power system stabilizers operating in a multi-machine power system including the uncertainty of model parameters. *Elsevier Appl. Math. Comput.* **2015**, *267*, 750–757. [CrossRef]
8. Liu, Z.; Yao, W.; Wen, J. Enhancement of Power System Stability Using a Novel Power System Stabilizer with Large Critical Gain. *Energies* **2017**, *10*, 449. [CrossRef]
9. Larsen, E.; Swann, D. Applying power system stabilizers part I: General concepts. *IEEE Trans. Power Appar. Syst.* **1981**, *6*, 3017–3024. [CrossRef]
10. Larsen, E.; Swann, D. Applying power system stabilizers part II: Performance objectives and tuning concepts. *IEEE Trans. Power Appar. Syst.* **1981**, *6*, 3025–3033. [CrossRef]
11. Larsen, E.; Swann, D. Applying power system stabilizers Part III: Practical considerations. *IEEE Trans. Power Appar. Syst.* **1981**, *6*, 3034–3046. [CrossRef]
12. Verdejo, H.; Torres, R.; Pino, V.; Kliemann, W.; Becker, C.; Delpiano, J. Tuning of controllers in power systems using a heuristic-stochastic approach. *Energies* **2019**, *12*, 2325. [CrossRef]
13. Zamee, M.A.; Won, D. Novel Mode Adaptive Artificial Neural Network for Dynamic Learning: Application in Renewable Energy Sources Power Generation Prediction. *Energies* **2020**, *13*, 405. [CrossRef]

14. Sokólski, P.; Rutkowski, T.A.; Ceran, B.; Horla, D.; Złotecka, D. Power System Stabilizer as a Part of a Generator MPC Predictive Control System. *Energies* **2021**, *14*, 6631. [CrossRef]
15. Verdejo, H.; Pino, V.; Kliemann, W.; Becker, C.; Delpiano, J. Implementation of Particle Swarm Optimization (PSO) Algorithm for Tuning of Power System Stabilizers in Multimachine Electric Power Systems. *Energies* **2020**, *13*, 2093. [CrossRef]
16. Nocoń, A.; Paszek, S.; Pruski, P. Multi-criteria optimization of the parameters of PSS3B system stabilizers operating in an extended power system with the use of a genetic algorithm. *Arch. Control Sci.* **2022**, *32*, 233–255.
17. Pruski, P.; Paszek, S. Location of generating units most affecting the angular stability of the power system based on the analysis of instantaneous power waveforms. *Arch. Control Sci.* **2020**, *30*, 273–293. [CrossRef]
18. *IEEE Standard 421.5*; IEEE Recommended Practice for Excitation System Models for Power System Stability Studies. IEEE: New York, NY, USA, 2016.
19. *IEEE Standard 421.2*; IEEE Guide for Identification, Testing, and Evaluation of the Dynamic Performance of Excitation Control Systems. IEEE: New York, NY, USA, 2014.
20. Izdebski, M.; Mazur, M. Współpraca cyfrowych układów wzbudzenia i regulacji napięcia z systemami automatyki elektrowni. EN: Cooperation of digital excitation and voltage regulation systems with power plant automation systems. In Proceedings of the VII Ogólnopolska Konferencja Zabezpieczenia Przekaźnikowe w Energetyce, Gdańsk, Poland, 6–8 October 2004.
21. Izdebski, M.; Poniatowski, M. *Opracowanie Układu Detekcji Przewodzenia Tyrystora w MOSTKU prostownikowym. EN: Design of a Thyristor Conduction Detection System in a Thyristor Rectifier Bridge*; Institute of Power Engineering: Warsaw, Poland, 2009; OG/212/09.
22. Izdebski, M. Innowacyjny algorytm pomiaru temperatury uzwojenia wirnika generatora. EN: Innovative algorithm for measuring the temperature of the generator rotor winding. *Energetyka* **2018**, *2*, 101–110, ISSN: 0013-7294.
23. Izdebski, M.; Kędra, B. Diesel-generator sets in islanded grids. In Proceedings of the 5th International Conference on Deregulated Electricity Market issues in South-Eastern Europe DEMSEE, Sitia, Greece, 23–24 September 2010.
24. *P100C-SX Instruction Manual*; Institute of Power Engineering: Warsaw, Poland, 2018. Available online: http://www.ien.gda.pl/files/page_files/138/p100c-sx-instruction-manual-rev22.pdf (accessed on 1 December 2022).
25. Małkowski, R.; Izdebski, M.; Miller, P. Adaptive algorithm of a controller of the transformer supplying the radial network reducing the risk of voltage collapse. *Energies* **2020**, *13*, 25. [CrossRef]
26. Bérubé, G.R.; Hajagos, L.M. *Accelerating-Power Based Power System Stabilizers*; Kestrel Power Engineering: Mississauga, ON, Canada, 2022. Available online: https://kestrelpower.com/Docs/PSS_Tutorial_Chapter_Accelerating_Power_R2.pdf?t= (accessed on 1 December 2022).
27. *IEEE Tutorial Course—Power System Stabilization via Excitation Control*; IEEE Power & Energy Society: Orlando, FL, USA, 2007.
28. *Reliability Guideline Power Plant Model Verification and Testing for Synchronous Machines*; NERC: Atlanta, GA, USA, 2018. Available online: https://www.nerc.com/comm/RSTC_Reliability_Guidelines/Reliability_Guideline_-_PPMV_for_Synchronous_Machines_-_2018-06-29.pdf (accessed on 1 December 2022).
29. Commission Regulation (EU) 2016/631 of 14 April 2016 establishing a network code on requirements for grid connection of generators (NC RfG). *Off. J. Eur. Union* **2016**, 1–68. Available online: https://op.europa.eu/en/publication-detail/-/publication/1267e3d1-0c3f-11e6-ba9a-01aa75ed71a1/language-en (accessed on 1 December 2022).
30. Nordic Grid Code 2007. *Nordic Collection of Rules*; NORDEL: Mölndal, Sweden, 2007.
31. *Guidance Notes for Synchronous Generators*; NGESO: Warwick, UK, 2019.
32. *Instrukcja Ruchu i Eksploatacji Sieci Przesyłowej. Warunki korzystania, Prowadzenia Ruchu, Eksploatacji i Planowania Rozwoju Sieci, EN: Instruction for the Transmission Network Operation and Maintenance. Terms of Use, Management, Operation and Planning of Network Development*; DPK-4320-1(4)/2011/LK; PSE SA: Warsaw, Poland, 2022.
33. *Power System Stabilizer Tuning Guidelines*; WECC: Salt Lake City, UT, USA, 2004. Available online: https://www.wecc.org/Reliability/PowerSystemStabilizerTuningGuidelines.pdf (accessed on 1 December 2022).
34. *WECC Power System Stabilizer Design and Performance Criteria*; WECC: Salt Lake City, UT, USA, 2004. Available online: http://rmpsinc.com/resources/WECC_PSS_Design_and_Performance_Criteria (accessed on 1 December 2022).
35. *Grid Code For Peninsular Malaysia*; Code/ST/ No. K0002/2016; Suruhanjaya Tenaga Energy Commission: Putrajaya, Malaysia, 2016.
36. *Generator Testing Guidelines. Testing Guidelines for Generators in TNB Grid System*; TNB (Tenaga Nasional Berhad): Kuala Lumpur, Malaysia, 2015.
37. *Power System Stabilizer (PSS) Tunin Guideline*; PDR_TPD GT 001/15 Rev.5; TNB (Tenaga Nasional Berhad): Kuala Lumpur, Malaysia, 2015.
38. Passive Band Pass Filter, AspenCore, Inc. 2022. Available online: https://www.electronics-tutorials.ws/filter/filter_4.html (accessed on 1 December 2022).
39. Izdebski, M. *Odtworzenie Układu Wzbudzenia Generatora Synchroniczn Nr 3 w Elektrowni Opole. Sprawozdanie z uruchomienia. EN: Retrofit of the Generator Excitation System No. 3 in the Opole Power Plant. Commissioning Report*; Institute of Power Engineering: Warsaw, Poland, 2017; OGC/177/17.
40. Izdebski, M. *Site Acceptance Test Procedure and Report of Kuala Langat Power Station*; Unit #13. AVR Retrofit Project; Commissioning Report. Malaysia; Institute of Power Engineering: Warsaw, Poland, 2017; OGC/123/17.

41. Izdebski, M.; Lubośny, W.; Zaranek, W. *Cyfrowy Regulator Napięcia Typu WGSY-300 do Generatora Synchronicznego Nr 12 w Elektrowni Bełchatów. Sprawozdanie z uruchomienia. EN: Digital Voltage Regulator WGSY-300 for the Synchronous Generator No. 12 in the Bełchatów Power Plant. Commissioning Report*; Institute of Power Engineering: Warsaw, Poland, 2015; OG/26/15.
42. Izdebski, M.; Sierak, S.; Mazur, M. *Układ Wzbudzenia i Regulacji Napięcia Typu WGSY-38 Generatora Nr 4 w Elektrowni Wodnej Żarnowiec. Sprawozdanie z uruchomienia. EN: Voltage Regulation System WGSY-38 for the Generator No. 4 in the Żarnowiec Hydro Power Plant. Commissioning Report*; Gdansk Division; Institute of Power Engineering: Warsaw, Poland, December 2008; OG/154/08.
43. Izdebski, M. *P400 AVR Ecitation System Upgrade*; Unit 2. Commissioning Report; Springerville Generating Station USA; Institute of Power Engineering: Warsaw, Poland, 2014; OG/321/14.
44. Izdebski, M. *Przegląd Okresowy Regulatora Napięcia Typu RNGA-63 oraz Stabilizatora Systemowego na Bloku Nr 3 w Energa Elektrownie Ostrołęka SA. EN: Periodic Inspection of the RNGA-63 Voltage Regulator and Power System Stabilizer on Unit 3 at Energa Elektrownie Ostrołęka SA*; Institute of Power Engineering: Warsaw, Poland, 2018; OG/252/18.
45. Izdebski, M.; Sierak, S. *P400 AVR Excitation System Parameters*; Commissioning Report; Louisa Generating Station. USA; Institute of Power Engineering: Warsaw, Poland, 2007; OGC/218/07.